Soft Matter

Accepted Manuscript

This is an *Accepted Manuscript*, which has been through the Royal Society of Chemistry peer review process and has been accepted for publication.

Accepted Manuscripts are published online shortly after acceptance, before technical editing, formatting and proof reading. Using this free service, authors can make their results available to the community, in citable form, before we publish the edited article. We will replace this *Accepted Manuscript* with the edited and formatted *Advance Article* as soon as it is available.

You can find more information about *Accepted Manuscripts* in the Information for Authors.

Please note that technical editing may introduce minor changes to the text and/or graphics, which may alter content. The journal's standard Terms & Conditions and the Ethical guidelines still apply. In no event shall the Royal Society of Chemistry be held responsible for any errors or omissions in this *Accepted Manuscript* or any consequences arising from the use of any information it contains.

ROYAL SOCIETY OF CHEMISTRY

www.rsc.org/softmatter

Micro and macrorheology at fluid-fluid interfaces

Joseph R. Samaniuk [a,*], *Jan Vermant* [a,b]

[a] *Department of Chemical Engineering, KU Leuven, University of Leuven, W. de Croylaan 46, bus 2423, Heverlee, 3001, Belgium*

[b] *Department of Materials, ETH Zürich, Vladimir Prelog weg 5, CH 8093 Zürich*

Abstract:

Interfacial transport phenomena play an important role in the dynamics of liquid interfaces found in emulsions, foams, and membranes. Both macroscopic and microscopic measurements of interfacial transport and rheology can be made, the former typically relying on the use of at least millimeter-scale probes, and the latter exploiting the motion of micrometer-scale probes. Recent publications have shown multiple orders of magnitude differences between experimentally observed diffusivities in passive microrheology, and the diffusivities expected based on macroscopic measurements of the surface rheology. In the present work, interfacial rheological measurements were made with both microrheological and macrorheological methods and the results are compared for different monolayers at an air-water interface. We have identified multiple aspects of particle-tracking microrheology that can contribute to orders-of-magnitude disagreement with macrorheological methods. In particular, unintentional tracking of particles not residing at the interface, the presence of large-scale interfacial heterogeneities, and underestimating static noise can all decrease estimates of surface viscosity from particle-tracking microrheology by orders of magnitude. After taking care to address these artifacts, we show that viscosities obtained from both methods agree well for poly(tertbutyl methacrylate) (PtBMA), and for dipalmitoylphosphatidylcholine (DPPC), but disagree by orders of magnitude for hexadecanol. In poly(tertbutyl acrylate) (PtBA), large-scale heterogeneities prevented us from obtaining representative surface viscosities. By making surface viscosity measurements in an interfacial stress rheometer (ISR) with needles of different aspect ratio, we show that compressibility or Marangoni stress related effects may be contributing to the orders of magnitude disagreement in micro and macrorheological measurements observed in the hexadecanol system.

* Corresponding author: *E-mail: joseph.samaniuk@cit.kuleuven.be*

Keywords:

Rheology, Interface, Microrheology, Particle tracking, Surfactant, Polymer

Introduction:

Liquid interfaces may have a surface viscoelasticity in addition to surface tension. It is clear that the behavior of so-called fluid-fluid interfaces is dependent on interfacial rheological properties and progress has been made in correlating rheological properties with observations of interfacial stability and transport [1-3]. Moreover, the seminal work of Saffman and Delbrück showed how the diffusion coefficient of membrane proteins is controlled by the surface viscosity, weakening the dependence of the diffusivity on the size of the objects compared to the bulk [4]. In recent years researchers from a variety of backgrounds have set out to characterize the viscosity and diffusivity of soft matter interfaces including simple monolayers and more complex assemblies. The most successful experimental devices developed for this purpose are designed for shear rheometry at constant surface area [5, 6], but there are methods designed for dilatational rheometry [7, 8]. Most of these devices can be considered macroscopic methods, in that they utilize probes or channels with dimensions of approximately millimeter scale or greater. They are typically designed such that the flow field is said to be viscometric, i.e., the kinematics are independent of the material function that is being investigated, enabling a clear-cut and model independent determination of the rheometrical functions.

Recently, so-called microrheological techniques have been used to measure interfacial shear viscosities [9-12]. Microrheology has advantages over macrorheology including smaller sample sizes, access to higher frequency ranges, the ability to measure small-scale material heterogeneities, and greater sensitivity. For these reasons, interfacial microrheology is well suited to the study of small, sensitive systems like biological membranes where the role of membrane fluidity and rheology has been recognized as a key feature. However, recent publications show interfacial shear viscosities measured with microrheology and macrorheology can differ by 3-4 orders of magnitude [13, 14]. These discrepancies suggest that there is a problem with either our understanding of fluid dynamics at liquid interfaces, the experimental techniques used in the literature, or a combination thereof. Understanding where this difference originates from is necessary if fundamental rheological properties are to be confidently extracted from passive microrheological results. Despite its many advantages, an encumbrance of microrheology is that the disturbance flow field generated by the moving probe is non-viscometric in nature. The flow generated by a translating probe at a rheologically complex

interface depends in a non-trivial manner on the different interfacial rheological material functions, possibly both in shear and dilation, exactly the values one is trying to extract from the particle displacement.

A number of methods and geometries have been developed to measure the rheological properties of liquid interfaces [15-20]. An important design consideration for all cases is the sensitivity of the device, often governed by the geometry of the probe. A macroscopic Boussinesq number (*Bo*) can be used to analyze the intrinsic sensitivity of the devices, which represents the relative contribution of surface viscous stresses to bulk viscous stresses, and can be written as:

$$Bo = \frac{\eta_s P/L'}{\eta_b A/L''} \quad (1)$$

where η_s is the interfacial viscosity, η_b is the bulk viscosity, P is the perimeter of the probe in contact with the interface, A is the area of the probe in contact with the bulk, and L' and L'' are the characteristic lengths over which the velocity of the fluid decays in the interface, and in the bulk phase, respectively. Of the macrorheological devices developed, the interfacial shear rheometer (ISR), which utilizes a ferromagnetic needle to deform the interface, is the most sensitive, and when taking the contributions of bulk flows into account can measure η_s as low as 10^{-6} Ns/m [21]. The small A/P values of micron-sized probes give microrheological methods increased sensitivity compared to macroscopic methods. Even surface viscosities as low as low as 10^{-11} Ns/m have been reported from particle tracking experiments [13].

The microrheological techniques can be categorized as either passive or active. In passive microrheology the position of a Brownian probe is recorded as a function of time, and the diffusivity of the probe is calculated from its mean squared displacement (*MSD*) [22]. In active microrheology the position of a probe is controlled with external force from equipment such as optical or magnetic tweezers [11, 23, 24]. Passive methods are appealing for their simplicity and, in the case of biological systems, for the prospect of tracking particles native to the system under investigation. Passive microrheology in bulk fluids has been successfully developed around the generalized Stokes-Einstein relation (GSER), which relates the diffusivity of Brownian particles to the complex rheological properties of the surrounding fluid. Under specific conditions, the GSER enables one to use microrheology to calculate rheological material functions that compare nicely with values obtained from conventional rheological equipment [23, 25].

For Brownian particles at interfaces, the assumptions behind the GSER are not generally met. The Einstein-Sutherland component of the GSER requires that the environment around the probe be incompressible, homogeneous, and isotropic. Since a probe at an interface experiences a compressible, anisotropic environment, microrheological measurements at interfaces may require a different approach. Relating the motion of a particle at an interface to the viscosity of the interface and the surrounding bulk fluids can be done with the use of hydrodynamic models. Saffman and Delbrück [4] proposed such a model in 1975. Their model describes the movement of a thin, disk-shaped probe embedded in an interface and undergoing Brownian motion. The constraints on the model require that $\eta_b \ell << \eta_s$ (ℓ is the length scale of the decay of fluid velocity), and that the interface be incompressible, assumptions that may be valid in the case of protein diffusion within lipid bilayers. However, these assumptions become problematic when extending the model to cases where the interface is less populated with interfacial objects or when the membrane layers become very fluid such that η_s and η_b are of the same order of magnitude, or to cases where the probe is large and extends into the bulk phases. Passive microrheology is often used under exactly these conditions, where micron-scale probes are embedded in interfaces of nanometer-scale thickness. Danov et al. [26] developed a model in which a probe at an interface may extend into the bulk fluids adjacent to the interface, and in which the interface may be considered compressible. A major concern for this model is the omission of Marangoni forces. Gradients in surface tension give rise to Marangoni forces that ultimately resist concentration gradients in interfacial molecules. Fischer et al. [27] generated a model in which a particle is allowed to extend into the bulk phases, and in which Marangoni forces are included. They present solutions to their model for drag coefficients on spherical particles at interfaces for the limiting cases where $Bo << 1$, and $Bo >> 1$. They assume the interface is incompressible and support that assumption by indicating that surface compression waves travel at much greater speed than a Brownian probe. In effect, they assert that Marangoni forces allow one to assume incompressibility. A notable feature of any model developed with the assumption of incompressibility is that it cannot admit contributions from dilatational flows.

Sickert and Rondelez [9] employed Danov et al.'s model [26] to report η_s for low surface coverages of *N*-palmitoyl-6-n-penicillanic acid (PPA), pentadecanoic acid (PDA), and *L*-α-dipalmitoylphosphatidylcholine (DPPC), each at an air-water interface. In follow-up work they

make corrections to their data based on the argument that interfaces, especially at low surface coverage, can be considered incompressible[28]. The authors compare hydrodynamic models from Danov et al. [26], Fischer et al. [27], and their own modified version of the two, and show that despite considerable disagreement among the models, all η_s values remain within the same order of magnitude. Bonales et al. [29] utilized the Danov et al. [26] model to calculate η_s values for poly(4-hydroxystyrene) (P4HS) at an air-water interface from particle tracking experiments, and compared results with those obtained from a canal viscometer. Over a range of four orders of magnitude, trends in η_s in both data sets agree nicely. However, η_s values from particle tracking are consistently 1-2 orders of magnitude lower than η_s from the canal viscometer. Better agreement between the canal viscometer and particle tracking experiments was reported by Hilles et al. [30], although many of the reported η_s values appear to exceed the upper-limit of passive particle tracking microrheology by an order of magnitude. Underestimates of η_s from microrheology as compared to macrorheological results are also reported by Ortega et al. [13]. The authors show 2-4 orders of magnitude disagreement in η_s in P4HS at an air-water interface for macro and microrheological results. They also show 4 to 8 orders of magnitude disagreement in micro and macrorheological results for PtBA at an air-water interface over a range of polymer molecular weight that spans four decades. The authors cannot explain these discrepancies and suggest that more experimental and theoretical work needs to be done. Maestro et al. [14] investigated the disagreement of micro and macrorheological data in the PtBA system and found that the results did not depend on model limitations, heterogeneity of the monolayer on the scale of the probe size, or the chemical nature of the probe. They suggest that experiments in an ISR where *Bo* is the controlled variable might tell us more about the nature of the difference between micro and macrorheological results.

Given the importance of diffusion of particles or proteins at interfaces, we seek to resolve the differences between macro- and microrheology at interfaces, to investigate the conditions under which the Saffman model and its variants [4] (relying on incompressibility of the interface) can be applied. A key aspect we intend to investigate is how the non-viscometric flow field in the microrheological experiment plays a role. To this end, we not only vary *Bo*, but also the aspect ratio of the magnetic rods used in the magnetic stress rheometer. We explore contributions of non-shear deformations to the flow fields by observing their effect on the measured force.

Methods:

Sample preparation

Samples of PtBA were obtained from Polymer Source Inc. (Montreal, QC, Canada), PtBMA and hexadecanol from Sigma-Aldrich, and DPPC from Avanti Polar Lipids (Alabaster, AL, USA). All samples were used as they were received. In the case of PtBA, PtBMA, and DPPC, solutions of the samples were prepared by dissolution in chloroform (VWR, Prolabo grade). The hexadecanol solution was prepared by dissolution in 2-propanol (VWR, Prolabo grade). All solutions were prepared with a concentration of approximately 0.1 mg/ml.

Polystyrene (PS) particles of 0.7 μm diameter with sulfonate functional groups were obtained as an 8 wt% aqueous dispersion from Invitrogen (Eugene, OR, USA). In particle-tracking experiments the particles were spread at the clean air-water interface with isopropanol as a spreading solvent. Thirty minutes were allowed between depositing particles and depositing the interfacial material. Spreading the interfacial material was done with a 50 μl syringe from Hamilton Company (Reno, NV, USA). In all experiments the subphase was filtered water from an Arium 611 having a resistivity of 18.2 MΩ-cm (Sartorius, Gottingen, Germany). After depositing the interfacial material, 30 minutes was allowed to pass before microscopy began or rheological test were performed.

Microrheology

Microrheological measurements were performed using a inverted microscope Olympus IX71 equipped with a VT-Hawk multiarray scanhead (Visitech) using a 60x oil-immersion objective under brightfield lighting. A custom Langmuir trough was designed and utilized that has a raised glass insert to allow for imaging of the interface with an objective working distance of 150 μm. Measurements were performed at 23^{o}C.

All image sequences were obtained at 30 frames per second for 200 frames with a C8800 Hamamatsu camera. Polystyrene (PS) particles of 0.7 μm diameter and contact angle of 90^{o} were used in all particle-tracking experiments[31]. In each image sequence, approximately 10-20 particles were tracked. Probe-probe interactions were avoided by tracking only the probes with

separation distances of at least 5 particle diameters. This distance was determined from control experiments where it was found that diffusivity did not depend significantly on probe-probe separation distance above this value.

Static noise was estimated by tracking particles deposited on the raised glass insert of the custom trough. Correction for static noise was made by subtracting the mean squared displacement (*MSD*) of the static-particle measurements from the *MSD* values obtained from tracking mobile particles. The diffusivity obtained from static noise was order 10^{-5} $\mu m^2/s$. Dynamic noise is not easily quantifiable, but its influence can be minimized by reducing the ratio between the exposure time for a single image, σ, and the lag time, τ. In all cases here, $\sigma/\tau = 0.09$, and having observed primarily diffusive behavior, i.e., *MSD* scaling with lag time to the first power, we can say from the analysis of Savin and Doyle [32] that we expect less than 3 % error in our microrheological measurement due to dynamic noise.

Matlab was used for particle tracking analysis. The code implemented to identify and track particles was originally developed by Crocker and Grier [22], and since modified and made available to the community [33]. Our own code was written to analyze particles tracks and to calculate *MSD* values, diffusivities, and η_s values. Mean square displacement values were obtained from tracking displacements between pairs of particles rather than the displacement of individual particles relative to a fixed coordinate system [9]. In two dimensions, this relative *MSD*, or MSD_{rel}, is related to diffusivity by

$$MSD_{\mathrm{rel}} \equiv \langle \Delta r_{\mathrm{rel}}^2(\tau) \rangle = 8Dt \qquad (2)$$

where r is the distance between a pair of particles, τ is the lag time, D is the diffusivity and t is time. In this way, collective motion of the particles is reduced or eliminated from the data which would otherwise result in erroneously large values of diffusivity. A time and ensemble average was used over all possible pairs of particles to calculate a representative MSD_{rel}.

The Fischer model [27] can be used to calculate surface viscosities from diffusivities, under the assumption that the interface is incompressible. In general, D is related to the drag on a particle by the Einstein-Sutherland relation

$$D = \frac{k_B T}{f} \tag{3}$$

where k_B is Boltzmann's constant, T is the absolute temperature and f is the hydrodynamic drag on the particle. In the limit where *Bo* >> 1, for a particle with cylindrical symmetry embedded at an interface with sub-phase viscosity, η_b, and a negligible upper-phase viscosity, the Fischer model expresses the translational drag coefficient as

$$f = \eta_b a \left(\frac{4\pi Bo}{\ln(Bo \cdot a/a_s) - \gamma}\right) \tag{4}$$

where γ is Euler's constant (0.5772), a is a characteristic length of the particle, and a_s is the radius of the cylindrical cross section of the particle at the interface. If the particle is a sphere, $a/a_s = \sin\theta$, where θ is the contact angle. In the limit where *Bo* << 1, for a sphere embedded in the interface, the Fischer model expresses the translational drag coefficient as an expansion in the *Bo* number as

$$f = \eta_b a \left(k^{(0)} + Bo \cdot k^{(1)} + o(Bo^2)\right) \tag{5}$$

where a is the sphere radius, and the coefficients of the expansion are fit with 3% accuracy as

$$k^{(0)} \approx 6\pi\sqrt{\tanh[32(d/a + 2)/(9\pi^2)]} \tag{6}$$

$$k^{(1)} \approx -4\ln\left(\frac{2}{\pi}\tan^{-1}\left(\frac{d+2a}{3a}\right)\right) \tag{7}$$

where d is the shortest distance from the apex of the particle to the level of the interface and takes a negative value when the particle is embedded in the interface (it takes a positive value when the particle is fully submerged in the subphase). In the case of a 90° contact angle, $d = -a$. In the gap between the limiting cases just described, approximately 0.1 < *Bo* < 10, we do not have a viable solution. However, if one boldly utilizes the result in the limit for *Bo* << 1 within the 0.1 < *Bo* < 10 regime, we can expect at least order-of-magnitude agreement with estimates of η_s calculated from an extrapolation of the two limiting solutions of the Fischer model. This is illustrated in Fig. 1, where the translational drag coefficients for both of these limiting cases are plotted as a function of *Bo* for a spherical particle with a 90° contact angle. In fact, if we were to use the Fisher model solution valid for *Bo* << 1 over the entire range of *Bo* shown in Fig. 1, we

would consistently *underestimate* η_s at high *Bo*, but always expect at least order-of-magnitude agreement with the Fischer model solution valid for *Bo* >> 1. This observation may explain the surprising agreement that Maestro et al. [14] found between different theoretical approaches for obtaining η_s, including the Fischer model valid for *Bo* << 1 that they utilized in the regime 0.1 < *Bo* < 100. In this work we utilize the *Bo* << 1 Fischer model solution in cases where *Bo* < 10. When *Bo* exceeds 10, the Fischer model solution valid for *Bo* >> 1 is utilized.

Maestro et al. [14] found that a scaling factor of 1.8 included in eq. (5) brought the Fischer model prediction for diffusivity of particles at a clean air-water interface in close agreement with their experimental observations. In our work the experimentally observed diffusivity of our particles at a clean air-water interface was 0.39 $\pm$ 0.09 $\mu m^2/s$, while the prediction from the Fischer model (90^o contact angle, 0.7 μm particles) is 0.53 $\mu m^2/s$. A scaling factor of 1.4 would bring the Fischer model prediction into better agreement with our experimentally-observed diffusivities, but this was not utilized in any of our data analysis. We note that the clean-interface diffusivity measured in our system agrees nicely with reports of diffusivities of PS particles at clean air-water interfaces reported in other studies [14, 28]. The supplementary file "Passive microrheology" is an interactive file that contains video from our particle-tracking experiments in combination with the corresponding values of probe diffusivity, η_s, and surface pressure, all as a function of surface coverage of DPPC.

Macrorheology

Macrorheological measurements were made with a magnetic rod interfacial shear rheometer (ISR) [17]. The device, the settings used, and the methods used to calculate η_s here have been described in great detail by Reynaert et al. [21]. For this particular study the open-ended glass channel used was 8 cm in length and 7.5 mm in width. Three needles of different length but of otherwise identical materials were prepared and treated with 5% dimethylchlorosilane in heptane solution. The contact angle of the needles at the air-water interface was 89 $\pm$ 3^o measured with a contact angle goniometer (CAM 200, KSV Instruments Finland). Surface viscosities are reported only for measurements with *Bo* > 100, where a linear velocity profile between the channel and the needle is a good assumption [34]. A low-frequency limit value of 0.05 Hz was used (see supplementary file "Low-Frequency Limit"), and strain was maintained below 1% for all

measurements. Measurement error here is stochastic in nature. Repeat measurements indicate that that error is approximately 10%, resulting in error bars smaller than figure symbols.

Results:

Experimental concerns in passive particle tracking

Identifying micron-size particles at an air-water interface with a microscope is simple when there are multiple particles within the field of view that are in the same focal plane. Invariably some of the particles deposited at the interface will enter the bulk phase and spend time near and adjacent to the interface without being adsorbed to it. Particle tracking algorithms identify particles based on their contrast with the surrounding medium, and it is common for the software to mistakenly identify a particle adjacent to the interface as one that is within it. The diligent experimentalist must check each tracked particle to be certain of its presence within the interface. An example of this is shown in Fig. 2, where the red lines indicate tracks of 0.7 μm PS particles at an air-water interface containing 2.1 mg/m^2 DPPC. The surface concentration of DPPC is high enough that Brownian motion is suppressed such that we clearly observe the collective, convective motion of the particles at the interface. In Fig 2a one of the tracked particles is not adsorbed to the interface and we observe the superposition of its Brownian and convective motion. The apparent η_s calculated from the tracking data in Fig. 2a is 3.4x10^{-8} Ns/m. In Fig 2b the particle adjacent to the interface has been removed from the tracking data and the apparent η_s is 9.1x10^{-5} Ns/m, three orders of magnitude larger. A video version of Fig 2b that reveals the subtle fluctuation of the rogue particle out of the focal plane has been included in the supplementary file "Figure 2b". Identifying tracked particles that are not at the interface is easy at high surface viscosities because of the suppressed Brownian motion of the particles adsorbed to the interface, as we see in Fig. 2. However, at low η_s the Brownian motion of the particles at the interface is often comparable to that of the particles in the bulk, and diligence is required to check each tracked particle for minor fluctuations out of the focal plane that expose it as a rogue.

One can only expect rheological material functions measured at the micron scale to agree with macroscopic measurements when the interfacial material behaves similarly as a continuum at both scales. It is known that heterogeneities within the interface can compromise microrheological measurements, especially when probe-interface interactions lead to local concentration gradients around the probe [10]. In the absence of probe-interface interactions, heterogeneities may exist in the interface simply by the nature of the interfacial material, and

how the material is spread. An example of this is shown in Fig. 3, where PtBA with a weight-average molecular weight of 39.5 kDa is spread at an air-water interface. In Fig. 3a-c, the images were obtained with a 60x oil-immersion objective under brightfield lighting. Images in Fig. 3d and 3e were obtained with a phase-contrast microscope with 20x and 4x air-objectives, respectively. Under brightfield lighting with the air-objectives, none of the structures observed in Fig. 3d-e were visible. The surface coverages in Fig. 3 vary between 1.2 and 1.6 mg/m^2 (see figure caption), but there are clearly concentration gradients in the interfacial material that result in heterogeneities with characteristic length scales from tens to hundreds of micrometers. One expects that tracking micron-scale particles that are homogeneously distributed in this interface will result in a broad range of particle diffusivities. However, we have observed with PtBA that in the presence of such interfacial heterogeneity, micron-scale particles may not distribute homogeneously in the interface, preferring to segregate to regions with low surface concentrations. This behavior is shown in Fig. 4 and within the supplementary video file "PtBA heterogeneities". There is a region of high surface coverage in the top right of Fig. 4, and a region of low surface coverage in the bottom left. The separation between the two regions is made clear from the presence of particles adsorbed to the interface at the boundary. Vigorous Brownian motion of the particles in the lower surface coverage region is clear in the supplementary video file, while the Brownian motion of the particles adsorbed to the boundary between the two regions is suppressed. The apparent η_s calculated from the particles in the low surface coverage region is 10^{-8} Ns/m, while those calculated from the particles adsorbed to the boundary between the two regions are order 10^{-5} Ns/m. An important observation is that the heterogeneities observed in Figs. 3-4 are not easily observed with a typical air-objective microscope under brightfield lighting. One may easily fail to recognize the inhomogeneity of the interface and, in the case of PtBA as shown in Fig. 4, ultimately report apparent η_s values that are lower than those obtained from macrorheological experiments by many orders of magnitude.

Static noise in particle tracking can be accounted for by subtracting the static-particle *MSD* from the *MSD* for particles at an interface. The decreased *MSD* results in lower estimates of particle diffusivity and ultimately larger estimates of η_s. As a consequence, underestimating static noise will lead to underestimates of η_s. The influence of static noise correction increases at higher surface viscosities where the signal from Brownian motion approaches the noise of the system.

As a result, underestimates of the static noise can alter the apparent trends in rheological materials functions as a function of surface pressure or surface coverage. An example of this behavior is shown in Fig. 5, where the apparent η_s is plotted as a function of surface coverage for hexadecanol at an air-water interface. The two sets of data come from a single experiment where static noise is corrected for in one set, and neglected in the other. Estimates of η_s are low when the static noise is not corrected for, and the underestimate becomes increasingly severe at higher surface coverages. The data point at 2.65 mg/m^2 in Fig. 5 has exceeded the upper limit of sensitivity for our passive particle tracking, but it is included here to demonstrate the increasing influence of static noise with increasing η_s.

Data from passive particle tracking can result in erroneous interfacial rheological material functions in certain circumstances that are often difficult for the very conscientious experimentalist to identify. It is well known that the effect of collective particle drift while observing an interface necessitates the use of a relative *MSD*, or MSD_{rel}, rather than a single-particle *MSD* [9, 14], and that particle-interface interactions can be a problem in certain systems. As discussed above, we have found that accidental tracking of particles adjacent to the interface, the presence of large interfacial heterogeneities, and underestimating static noise may each result in negative errors in rheological data that are often many orders in magnitude.

Comparing micro and macrorheological data

Macrorheological data obtained with the ISR on PtBMA, hexadecanol, and DPPC at an air-water interface are shown in Fig. 6. The low frequency limit of the modulus of the complex viscosity, $|\eta_s^*|$, is plotted as a function of Π for the three systems, and all of the data follow power-law scaling that agree well with macrorheological data in other studies [35-37].

Micro and macrorheological data agree nicely in both the PtBMA system and the DPPC system and the two approaches show substantial overlap. Surface viscosity for PtBMA as a function of surface coverage is shown in Fig. 7, where both the magnitude and trend of each data set agree well. The result is a set of data revealing an increase in η_s of six orders of magnitude with a change of 0.7 mg/m^2 surface coverage. Similar results are shown in Fig. 8 for DPPC. There is considerable overlap in the data in the case of DPPC that reveals excellent agreement in both magnitude and trend. Again, the two data sets combined reveal an increase in η_s that spans five

orders of magnitude with a change of 0.6 mg/m^2 surface coverage. The Cox-Merz rule is an empirical finding for simple fluids where the shear viscosity is equal to the complex viscosity over a wide range of shear rates and frequencies. Although it is tempting to draw conclusions about the applicability of the Cox-Merz rule in the PtBMA and DPPC systems, correspondence with Cox-Merz is not necessary for the agreement seen in Figs. 7 and 8 since passive microrheology is intrinsically done within the linear viscoelastic regime of the fluid, and macrorheological measurements are made in the low-frequency limit. In effect, η_s from both methods may be considered a zero shear viscosity that we expect to agree regardless of the applicability of Cox-Merz.

Estimates of η_s from micro and macrorheological experiments did not agree well in the hexadecanol system, as seen in Fig. 9, where apparent η_s is plotted as a function of surface coverage for both techniques. There is disagreement in both magnitude and trend, with microrheological results many orders of magnitude lower than the macrorheological results. Thus, the Brownian motion of the microscopic particles is faster than would be expected when the deformation field around the particle is dominated by simple shear. The experimental concerns discussed earlier were diligently eliminated as possible contributors to this disagreement, and it is informative to point out that the trends in η_s with Γ for microrheological data for PtBMA, hexadecanol, and DPPC are all similar (Figs. 7-9). In each instance η_s scales with Γ to the 20th power, approximately, suggesting that domain formation in hexadecanol at an air-water interface [36] is unlikely to be responsible since similar domains also form in DPPC at an air-water interface [37].

One of the assumptions in the Fischer model [27] used to calculate η_s in this work is that the interface is incompressible and, implicitly, they assume that there is no significant dilatational viscoelasticity. The very good to excellent agreement between both measurement techniques in PtBMA and DPPC in Figs. 7 and 8 suggest that, at least in those systems, the assumption holds, and the shear viscosity of the monolayer can be expected to dominate the damping of the movement of the probe particle. The disagreement of the data in the hexadecanol system requires that previous assumptions be tested, including the assumption of incompressibility, and the assumption that out-of-plane motions are not present, or are negligible. One way to evaluate the influence of compressibility is to introduce a mixed flow field with both shear and extensional

contributions where the effects of local dilation and compression may be manifest. This can be done in an ISR by varying the aspect ratio of the probe needle for the purpose of introducing more or less of the extensional or dilatational flow present at both ends of the needle.

Three needles of different aspect ratio were fabricated and used to test the PtBMA, hexadecanol, and DPPC systems. Table 1 includes the physical dimensions of the needles and shows that aspect ratio was varied by varying only needle length. Results of experiments completed in the hexadecanol system are shown in Fig. 10, where the apparent $|\eta_s^*|$ is plotted as a function of Π. Dependence of the modulus of the apparent η_s^* on Π increases with decreasing needle aspect ratio. Solid lines are power-law fits of the form:

$$|\eta_s^*| = a\Pi^b \tag{8}$$

Values for the exponent b are plotted in Fig. 11 as a function of needle aspect ratio for all three of the systems examined. Error bars represent a single standard deviation based on the regression statistics. For the hexadecanol system, b increases markedly with decreasing aspect ratio. For DPPC the increase is much less pronounced, and for PtBMA there is a slight decrease with decreasing aspect ratio. In their simulations of incompressible interfaces, Levine et al. [38] showed that when probe dimensions are smaller than the length scale $\ell_o = \eta_s/\eta_b$, where η_b is the bulk viscosity, the drag coefficients on a translating probe are expected to be independent of the aspect ratio of the probe. In our experiments the needle length is always less than ℓ_o, putting our results well within the regime where drag is not expected to depend on probe aspect ratio in an incompressible interface.

The strong dependence of η_s on needle aspect ratio in the hexadecanol system suggests that dilatational contributions may be present. The details concerning why dilatational flow might result in the data shown in Fig. 11 are unclear. Elfring et al. [39] recently showed with simulations that introducing dilatational contributions can have remarkably non-intuitive consequences for drag coefficients on translating probes at interfaces. In particular, increasing the magnitude of shear viscosity in the case of a probe translating through an insoluble surfactant interface increased the magnitude of the Marangoni forces. Verwijlen et al. [40] discussed the dynamics of an extensional interfacial rheometer in the context of the governing transport equations and showed that the measured forces can vary dramatically depending on the balance between

resistances to shear and dilatational deformations. A similar analysis is helpful here, and we start by utilizing the Boussinesq-Scriven constitutive model for Newtonian interfaces [41]

$$\mathbf{T}_s = [\gamma + (\kappa_s - \eta_s)\nabla \cdot \boldsymbol{\nu}_s]\mathbf{I} + 2\eta_s \mathbf{D}_s \tag{9}$$

where γ is the surface tension, κ_s is the dilatational viscosity, $\boldsymbol{\nu}_s$ is the surface velocity vector, and $\mathbf{D}_s$ is the surface deformation tensor. The equation of interfacial momentum transport [42] can be written as

$$-\mathbf{n} \cdot \|\mathbf{P}\| = \mathbf{F}^S + \boldsymbol{\nabla}_S \cdot \mathbf{P}^S \tag{10}$$

where $\mathbf{n}$ is a unit vector normal to the interface, $\mathbf{P}$ is the stress tensor in the bulk phase, $\mathbf{F}^S$ is the surface-excess force density vector, and $\mathbf{P}^S = \mathbf{I}\gamma + \mathbf{T}_S$. Equations (9) and (10) combined give the governing equations for a Newtonian, two-dimensional interface that, for the case of large *Bo*, can be written as

$$\frac{\partial \gamma}{\partial x} + \frac{\kappa_s}{2}\left(\frac{\partial^2 v_x}{\partial x^2} + \frac{\partial^2 v_y}{\partial x \partial y}\right) + \frac{\eta_s}{2}\left(2\frac{\partial^2 v_x}{\partial y^2} + \frac{\partial^2 v_x}{\partial x^2} - \frac{\partial^2 v_y}{\partial x \partial y}\right) = 0 \tag{11a}$$

$$\frac{\partial \gamma}{\partial y} + \frac{\kappa_s}{2}\left(\frac{\partial^2 v_y}{\partial y^2} + \frac{\partial^2 v_x}{\partial y \partial x}\right) + \frac{\eta_s}{2}\left(2\frac{\partial^2 v_y}{\partial x^2} + \frac{\partial^2 v_y}{\partial y^2} - \frac{\partial^2 v_x}{\partial y \partial x}\right) = 0 \tag{11b}$$

It is informative to rewrite the first term of Eqs. (11a) and (11b) in terms of surface concentration, Γ, and to introduce dimensionless variables. The first term in eqns. (11a) and (11b) can be rewritten as

$$\frac{\partial \gamma}{\partial x} = \frac{\partial \gamma}{\partial \Gamma}\frac{\partial \Gamma}{\partial x} = E_\pi \frac{\partial \Gamma}{\partial x} \tag{12a}$$

$$\frac{\partial \gamma}{\partial y} = \frac{\partial \gamma}{\partial \Gamma}\frac{\partial \Gamma}{\partial y} = E_\pi \frac{\partial \Gamma}{\partial y} \tag{12b}$$

where E_π is a linearization of the equation of state for $\gamma = f(\Gamma)$, close to the nominal surface concentration of the system, Γ_0. In combination with the dimensionless variables: $\bar{\Gamma} = \frac{\Gamma}{\Gamma_0}$, $\bar{v}_x = \frac{v_x}{\dot{\gamma} x_0}$, $\bar{v}_y = \frac{v_y}{\dot{\gamma} y_0}$, $\bar{x} = \frac{x}{x_0}$, $\bar{y} = \frac{y}{x_0}$, eqns. (11a) and (11b) can be rewritten in the form

$$Ma\frac{\partial\bar{\Gamma}}{\partial\bar{x}} + \frac{\theta}{2}\left(\frac{\partial^2\bar{v}_x}{\partial\bar{x}^2} + \frac{\partial^2\bar{v}_y}{\partial\bar{x}\partial\bar{y}}\right) + \frac{1}{2}\left(2\frac{\partial^2\bar{v}_x}{\partial\bar{y}^2} + \frac{\partial^2\bar{v}_x}{\partial\bar{x}^2} - \frac{\partial^2\bar{v}_y}{\partial\bar{x}\partial\bar{y}}\right) = 0 \quad (13a)$$

$$Ma\frac{\partial\bar{\Gamma}}{\partial\bar{y}} + \frac{\theta}{2}\left(\frac{\partial^2\bar{v}_y}{\partial\bar{y}^2} + \frac{\partial^2\bar{v}_x}{\partial\bar{y}\partial\bar{x}}\right) + \frac{1}{2}\left(2\frac{\partial^2\bar{v}_y}{\partial\bar{x}^2} + \frac{\partial^2\bar{v}_y}{\partial\bar{y}^2} - \frac{\partial^2\bar{v}_x}{\partial\bar{y}\partial\bar{x}}\right) = 0 \quad (13b)$$

where $Ma \equiv \frac{E_\pi\Gamma_0}{\eta_s\dot{\gamma}}$ is defined as the Marangoni number, and $\theta \equiv \frac{\kappa_s}{\eta_s}$ is the ratio of the surface dilatational viscosity to the surface shear viscosity. As the disturbance flow field for a Brownian particle is non-viscometric, the relative magnitude of the dimensionless groups, which contain the material functions, will determine the nature of the disturbance velocity field. The influence of dilatation on the flow behavior is captured in two dimensionless groups. The Marangoni number represents an elastic resistance to dilatation, and θ represents a viscous resistance to dilatation. Large values of both *Ma* and θ mean there is great resistance to dilatational flows such that shear deformations are expected to dominate. However, the value of each group can vary independently, and the relative values have consequences for the response of the system. For example, a small value of *Ma* and a large value of θ would be found in a system that undergoes dilatation with great resistance, but does not respond quickly to the presence of surface concentration gradients. Once dilatation is induced, it is slow to recover. A large value of *Ma* and a small value of θ would be found in a system that undergoes dilatation with ease, but responds rapidly to the presence of surface concentration gradients. Any dilatation induced is rapidly quenched. The experiments utilizing needles of varied aspect ratio do not alter values of *Ma* and θ, rather they attenuate the terms in eqns. (13a) and (13b) associated with them. In the case of an infinitely long needle, eqns. (13a) and (13b) reduce to those associated with simple shear. For short needles, the terms containing *Ma* and θ become quite relevant. Values of *Ma* number for the interfaces examined here vary many orders of magnitude with changes in surface coverage. Accurate measurements of κ_s are a difficult to obtain, but values of θ will vary with surface coverage as well. Table 2 contains approximate or order-of-magnitude estimates of E_π, η_s, κ_s, *Ma*, and θ for the three systems at $\Gamma_0 \sim 1.2\ \mathrm{mg/m^2}$. Marangoni number is lowest in hexadecanol, and the ratio Ma/θ is also the smallest of the three systems. The Fischer model assumes interfaces are incompressible based on the assertion that the time scale for rearrangement of the interface is much smaller than the time scale for the movement of the probe. As *Ma* decreases, the time scale for interfacial rearrangement increases and, as it

approaches the time scale for the movement of the probe, the assumption of incompressibility and the consequent absence of Marangoni stresses becomes questionable. The significance of both Ma and θ makes it difficult to draw hard conclusions, but this order-of-magnitude analysis is at least consistent with the assertion that the relative magnitudes of Ma and θ differ in the three systems examined, and that those differences are in the direction expected when dilatational effects are significant. Although they are unexpected, it is worth noting that out-of-plane components, especially those induced by local dilation or compression, might also influence η_s measurements from needles of varied aspect ratio. Our understanding of the results is still developing, but it is encouraging to see that the trend of increasing b with decreasing aspect ratio is in the direction of the microrheology data, where probes of aspect ratio unity were used and η_s scales with Π to the 20^{th} power, approximately. Future work will focus on a combination of flow visualization and computational simulations in order to improve our understanding of this and to clarify correlations between the material parameters E_π, η_s, and κ_s, and interfacial rheological behavior in such a way that one can predict when discrepancies between micro- and microrheological methods will arise.

Conclusions:

We have presented and compared microrheological and macrorheological data for PtBMA, DPPC, and hexadecanol, each at an air-water interface. Experimental concerns for passive microrheology that can easily be overlooked and that can result in underestimates of surface viscosity are discussed. These include the tracking of particles not residing at the interface, large-scale heterogeneities of the interfacial material, and the influence of static noise, all of which may help explain disagreements in micro and macrorheological data reported in the literature that are multiple orders in magnitude. Having addressed these concerns, we show that micro and macrorheological data are in excellent agreement for the PtBMA and DPPC systems, but that there is a large disagreement within the hexadecanol system. Large-scale heterogeneities of the interface inhibited reliable microrheological data acquisition in PtBA, which may explain the discrepancies between micro-and macrorheology reported in literature. We have also presented evidence that dilatational effects may play a role in the disagreement of micro- and macrorheological data in hexadecanol. Drag coefficients for a probe in an incompressible interface under the same conditions as our experiments are not expected to depend on probe aspect ratio, but we have observed a dependence of surface viscosity on needle aspect ratio in an ISR in the hexadecanol system. We have discussed the results within the framework of the governing transport equations and relevant non-dimensional groups and indicated where dilatational effects may influence the rheological measurements in hexadecanol.

Acknowledgements:

The authors are grateful for the thoughtful input of Prof. Gerald G. Fuller (Stanford University) that certainly improved the quality of this work. This project was supported by a Pegasus Marie Curie Fellowship from the Belgian science foundation Fonds Wetenschappelijk Onderzoek (FWO), and in part by the Hercules foundation - Flanders (HER/08/21).

References:

1. D. Langevin, *Adv. Colloid Interface Sci.*, 2000, **88**, 209-222.
2. P. Erni, P. Fischer, V. Herle, M. Haug and E. J. Windhab, *Chemphyschem*, 2008, **9**, 1833-1837.
3. D. Leiske, C. Leiske, M. Toney, M. Senchyna, H. Ketelson, D. Meadows, S. Srinivasan, L. Jones and G. G. Fuller, *Biophys. J.*, 2012, **102**, 719-719.
4. P. G. Saffman and M. Delbruck, *Proc. Natl. Acad. Sci. U. S. A.*, 1975, **72**, 3111-3113.
5. G. G. Fuller and J. Vermant, *Annu. Rev. Chem. Biomol. Eng.*, 2012, **3**, 519-543.
6. R. Miller and L. Liggieri, *Interfacial Rheology*, Brill, 2009.
7. T. Verwijlen, P. Moldenaers and J. Vermant, *Eur. Phys. J-Spec. Top.*, 2013, **222**, 83-97.
8. S. C. Russev, N. Alexandrov, K. G. Marinova, K. D. Danov, N. D. Denkov, L. Lyutov, V. Vulchev and C. Bilke-Krause, *Rev. Sci. Instrum.*, 2008, **79**, 10.
9. M. Sickert and F. Rondelez, *Phys. Rev. Lett.*, 2003, **90**.
10. V. Prasad, S. A. Koehler and E. R. Weeks, *Phys. Rev. Lett.*, 2006, **97**.
11. P. Dhar, Y. Y. Cao, T. M. Fischer and J. A. Zasadzinski, *Phys. Rev. Lett.*, 2010, **104**, 4.
12. S. Q. Choi, S. Steltenkamp, J. A. Zasadzinski and T. M. Squires, *Nat. Commun.*, 2011, **2**, 6.
13. F. Ortega, H. Ritacco and R. G. Rubio, *Curr. Opin. Colloid In.*, 2010, **15**, 237-245.
14. A. Maestro, L. J. Bonales, H. Ritacco, T. M. Fischer, R. G. Rubio and F. Ortega, *Soft Matter*, 2011, **7**, 7761-7771.
15. R. J. Myers and W. D. Harkins, *J. Chem. Phys.*, 1937, **5**, 601-603.
16. S. G. Oh and J. C. Slattery, *J. Colloid Interf. Sci.*, 1978, **67**, 516-525.
17. C. F. Brooks, G. G. Fuller, C. W. Frank and C. R. Robertson, *Langmuir*, 1999, **15**, 2450-2459.
18. S. Vandebril, A. Franck, G. G. Fuller, P. Moldenaers and J. Vermant, *Rheol. Acta*, 2010, **49**, 131-144.
19. R. Miller, R. Wustneck, J. Kragel and G. Kretzschmar, *Colloid Surf. A-Physicochem. Eng. Asp.*, 1996, **111**, 75-118.
20. R. S. Ghaskadvi and M. Dennin, *Rev. Sci. Instrum.*, 1998, **69**, 3568-3572.
21. S. Reynaert, C. F. Brooks, P. Moldenaers, J. Vermant and G. G. Fuller, *J. Rheol.*, 2008, **52**, 261-285.
22. J. C. Crocker and D. G. Grier, *J. Colloid Interf. Sci.*, 1996, **179**, 298-310.

23. T. M. Squires and T. G. Mason, *Annu. Rev. Fluid Mech.*, 2010, **42**, 413-438.
24. C. Y. Park, H. D. Ou-Yang and M. W. Kim, *Rev. Sci. Instrum.*, 2011, **82**, 8.
25. T. G. Mason and D. A. Weitz, *Phys. Rev. Lett.*, 1995, **74**, 1250-1253.
26. K. Danov, R. Aust, F. Durst and U. Lange, *J. Colloid Interf. Sci.*, 1995, **175**, 36-45.
27. T. M. Fischer, P. Dhar and P. Heinig, *J. Fluid Mech.*, 2006, **558**, 451-475.
28. M. Sickert, F. Rondelez and H. A. Stone, *Epl*, 2007, **79**.
29. L. J. Bonales, H. Ritacco, J. E. F. Rubio, R. G. Rubio, F. Monroy and F. Ortega, *TOPCJ*, 2007, **1**, 25-32.
30. H. M. Hilles, H. Ritacco, F. Monroy, F. Ortega and R. G. Rubio, *Langmuir*, 2009, **25**, 11528-11532.
31. S. Coertjens, P. Moldenaers, J. Vermant and L. Isa, *Langmuir*, 2014, doi: 10.1021/la500888u.
32. T. Savin and P. S. Doyle, *Biophys. J.*, 2005, **88**, 623-638.
33. D. Blair and E. Dufresne, The Matlab particle tracking code repository, physics.georgetown.edu/matlab/, downloaded 2013.
34. T. Verwijlen, P. Moldenaers, H. A. Stone and J. Vermant, *Langmuir*, 2011, **27**, 9345-9358.
35. M. Sacchetti, H. Yu and G. Zografi, *Langmuir*, 1993, **9**, 2168-2171.
36. G. T. Gavranovic, R. E. Kurtz, K. Golemanov, A. Lange and G. G. Fuller, *Ind. Eng. Chem. Res.*, 2006, **45**, 6880-6884.
37. E. Hermans and J. Vermant, *Soft Matter*, 2014, **10**, 175-186.
38. A. J. Levine, T. B. Liverpool and F. C. MacKintosh, *Phys. Rev. Lett.*, 2004, **93**, 4.
39. G. J. Elfring, L. G. Leal and T. Squires, Paper: "Interfacial dilatational rheology" presented at the Society of Rheology annual meeting, Montreal, QC, Canada, 2013.
40. T. Verwijlen, D. L. Leiske, P. Moldenaers, J. Vermant and G. G. Fuller, *J. Rheol.*, 2012, **56**, 1225-1247.
41. L. E. Scriven, *Chem. Eng. Sci.*, 1960, **12**, 98-108.
42. D. A. Edwards, H. Brenner and D. T. Wasan, *Interfacial Transport Processes and Rheology*, Butterworth-Heinemann, Boston, 1991.

Tables:

Aspect ratio	Thickness (μm)	Length (mm)	Weight (g)
26.5	170	4.5	0.0003
82.4	170	14.0	0.0012
153	170	26.0	0.0016

Table 1. Dimensions of the magnetic needles used in measurements with the interfacial shear rheometer.

Material	Γ_0 (mg/m^2)	$E_\pi\Gamma_0$ (kg/s^2)	η_s (Ns/m)	κ_s (Ns/m)	Ma	θ	Ma/θ
Hexadecanol	1.3	0.04	10^{-4}	10^{0}	400	10^{4}	0.04
DPPC	1.2	0.08	10^{-5}	10^{0}	8,000	10^{5}	0.08
PtBMA	1.3	0.05	10^{-4}	10^{-1}	500	10^{3}	0.5

Table 2. Parameter and dimensionless group estimates for the hexadecanol, DPPC, and PtBMA systems.

Figures:

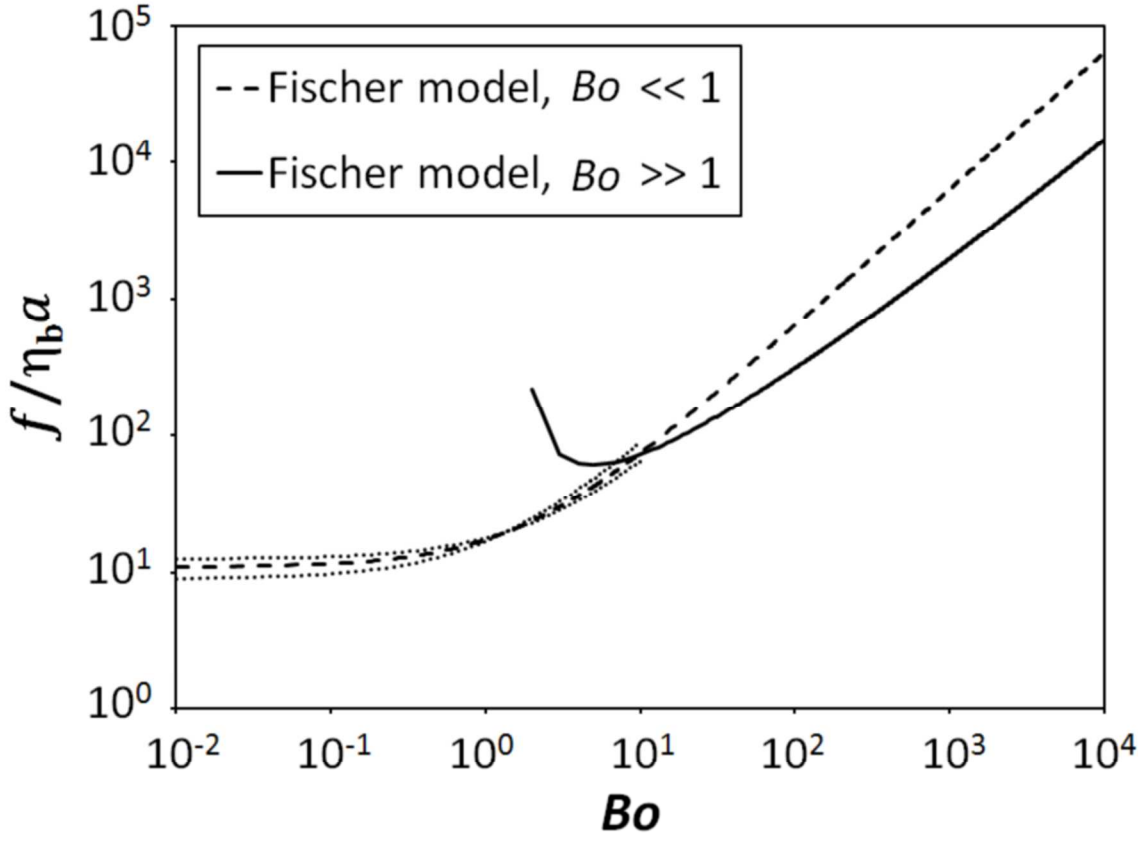

Figure 1. Translational drag coefficients for a spherical particle embedded at an interface with a contact angle of 90°, calculated from the Fischer model in the limits $Bo \ll 1$ and $Bo \gg 1$, plotted as a function of Bo. Utilizing the form of the Fischer model valid at low Bo in the regime $0.1 < Bo < 100$ will give values that are in order-of-magnitude agreement with those obtained by extrapolating the two limiting solutions together. Utilizing the Fischer model valid for $Bo \ll 1$ at higher surface viscosities ($Bo > 10$), will provide underestimates of Bo, and η_s. The dotted lines above and below the dashed line are values from the Fischer model (valid for $Bo \ll 1$) for contact angles of 70° and 110°, and are shown to indicate the relatively small deviations introduced by error in one's estimate of contact angle. For the Fischer model valid for $Bo \gg 1$, the same values (70° and 110° contact angles) deviated from the values obtained with a 90° contact angle by less than 2.5 %.

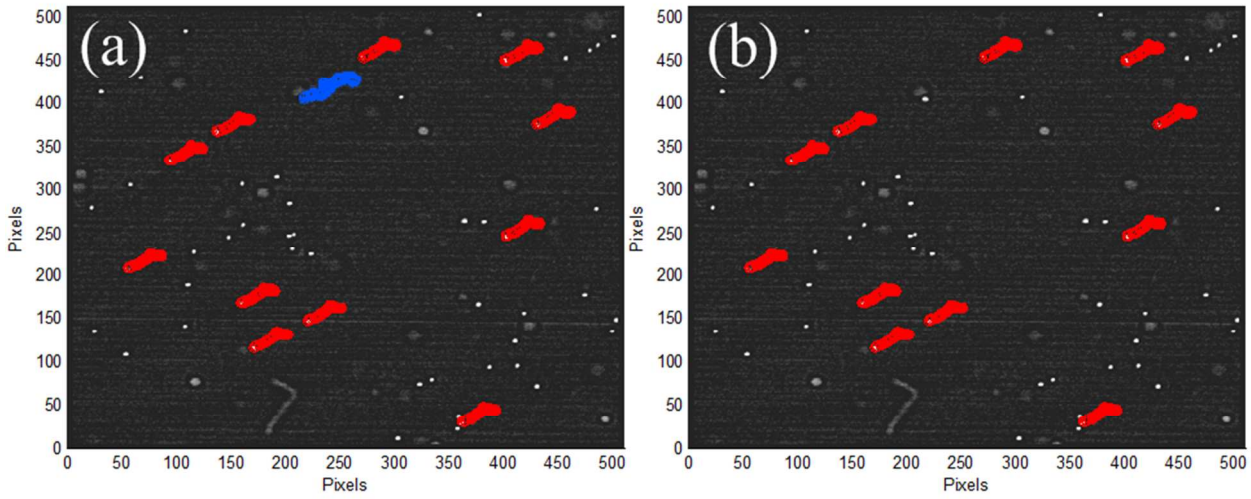

Figure 2. Tracks of 0.7 μm PS particles at an air-water interface (red) with 2.1 mg/m^2 DPPC. In (a), a single tracked particle (blue) is adjacent to the interface. This is clearly seen from its discordant track and confirmed by observing its subtle fluctuations out of the focal plane. The apparent η_s calculated from the tracks in (a) is 3.4x10^{-8} Ns/m. In (b) the rogue particle has been removed from the tracking data and the apparent η_s is 9.1x10^{-5} Ns/m. A video version of Fig. 2b can be found in the supplementary file: "Figure 2b".

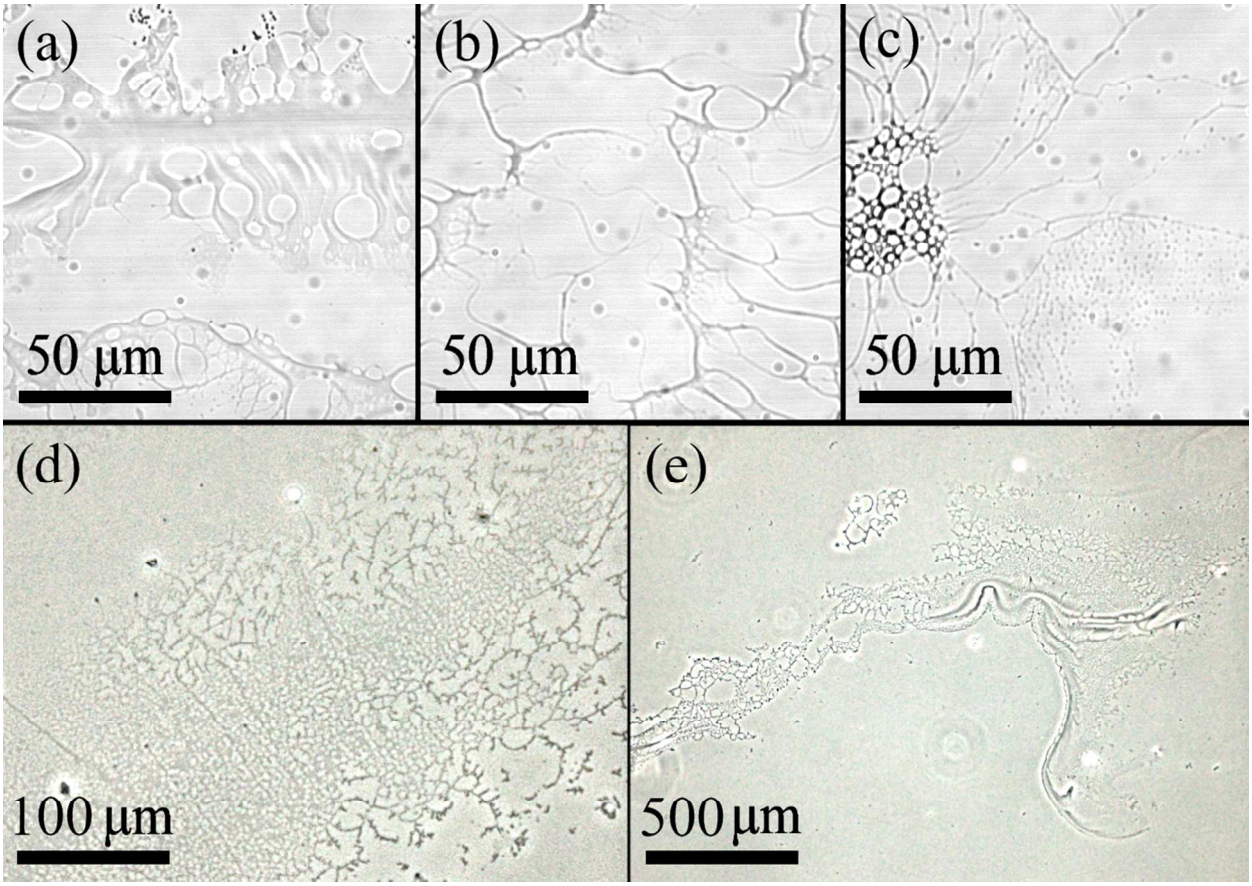

Figure 3. Heterogeneities in PtBA spread at an air-water interface. Images (a), (b), and (c) were taken with the 60x oil-immersion objective, at surface coverages of 1.26 mg/m^2 (12.0 mN/m), 1.5 mg/m^2 (23.0 mN/m), and 1.26 mg/m^2, respectively. Images (d) and (e) were obtained with a phase-contrast microscope with 20x and 4x air-objectives, respectively. Surface coverage in (d) and (e) was 1.65 mg/m^2. Under brightfield lighting with the air-objectives, none of the structures in (d) and (e) were visible.

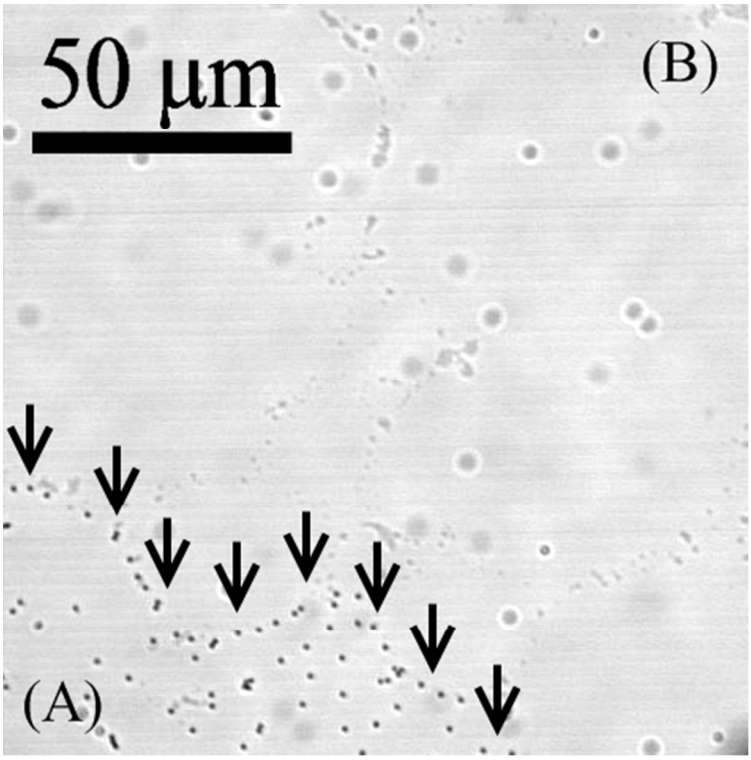

Figure 4. Image of PtBA at an air-water interface with 0.7 µm PS particles adsorbed to the interface in the bottom left. The surface coverage of PtBA varies sharply, with a region of low coverage in the bottom left of the image, (A), and a region of high coverage in the upper and right-most parts of the image, (B). A line of particles trapped at the boundary of these regions is indicated with arrows. The difference in Brownian motion between the particles in the low-coverage region and the particles trapped at the boundary between the two regions is clearly seen in the video included in the supplementary data entitled "PtBA heterogeneities".

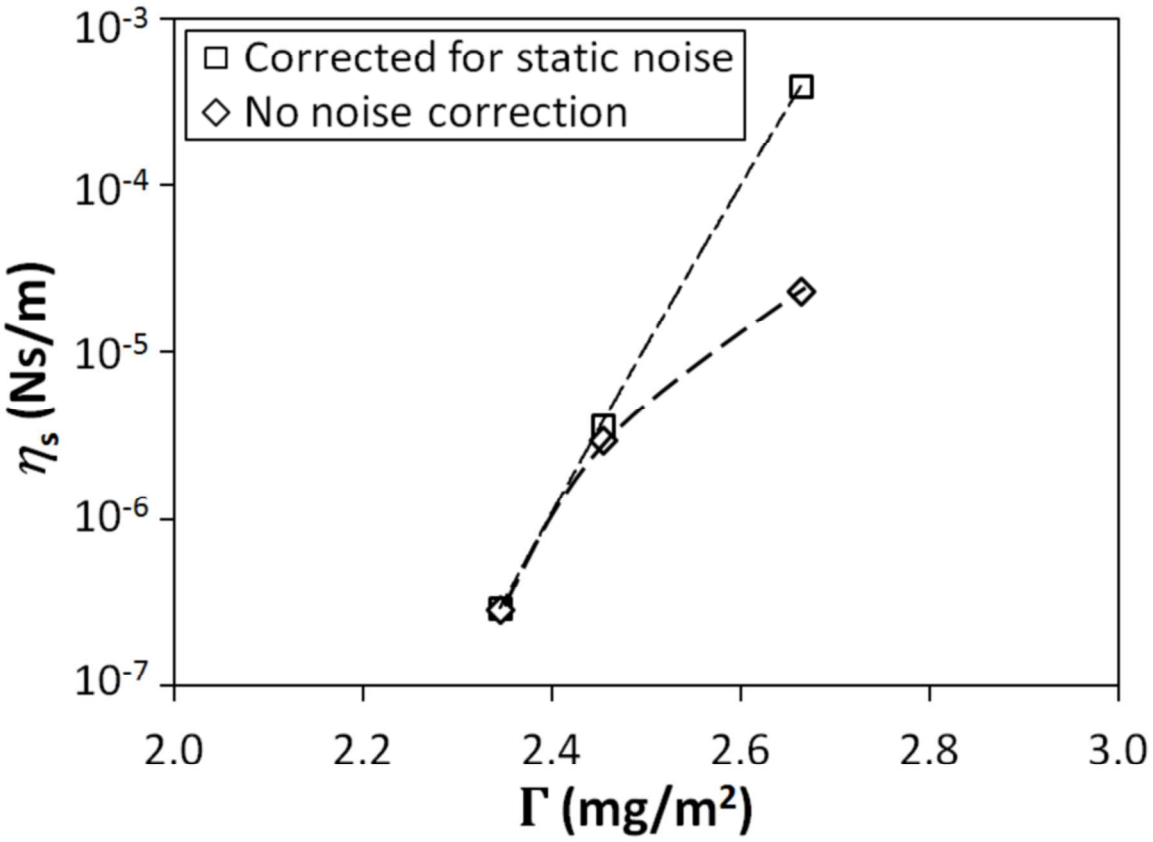

Figure 5. Surface viscosity as a function of surface coverage from particle tracking experiments with hexadecanol at an air-water interface. Square data points represent data that includes the correction for static noise, diamond symbols represent the same data points without any correction for static noise. Dashed lines are to guide the eye and emphasize the difference in apparent trend.

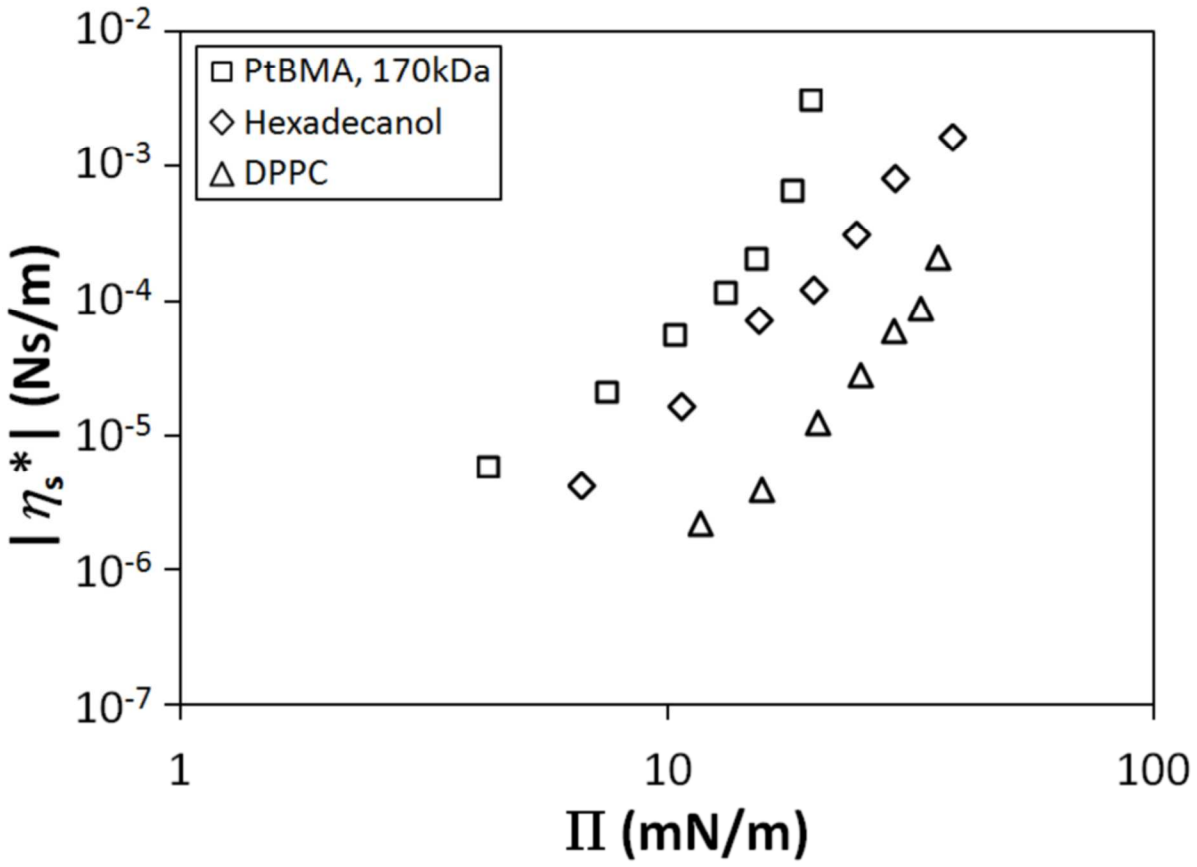

Figure 6. Modulus of η_s^* as a function of surface pressure measured with the ISR for PtBMA (170 kDa), hexadecanol, and DPPC at an air-water interface in the low-frequency limit.

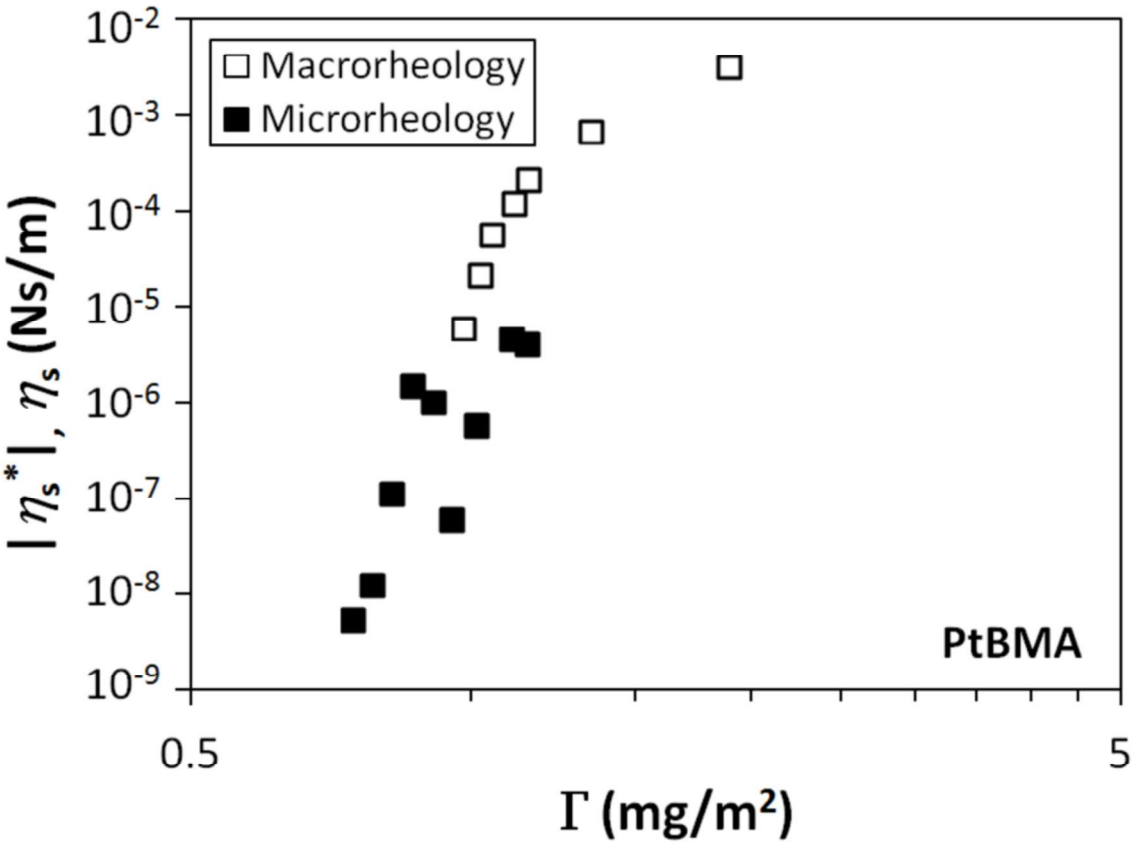

Figure 7. Surface viscosity as a function of surface coverage for PtBMA. Microrheological results (■) agree well with macrorheological results (□).

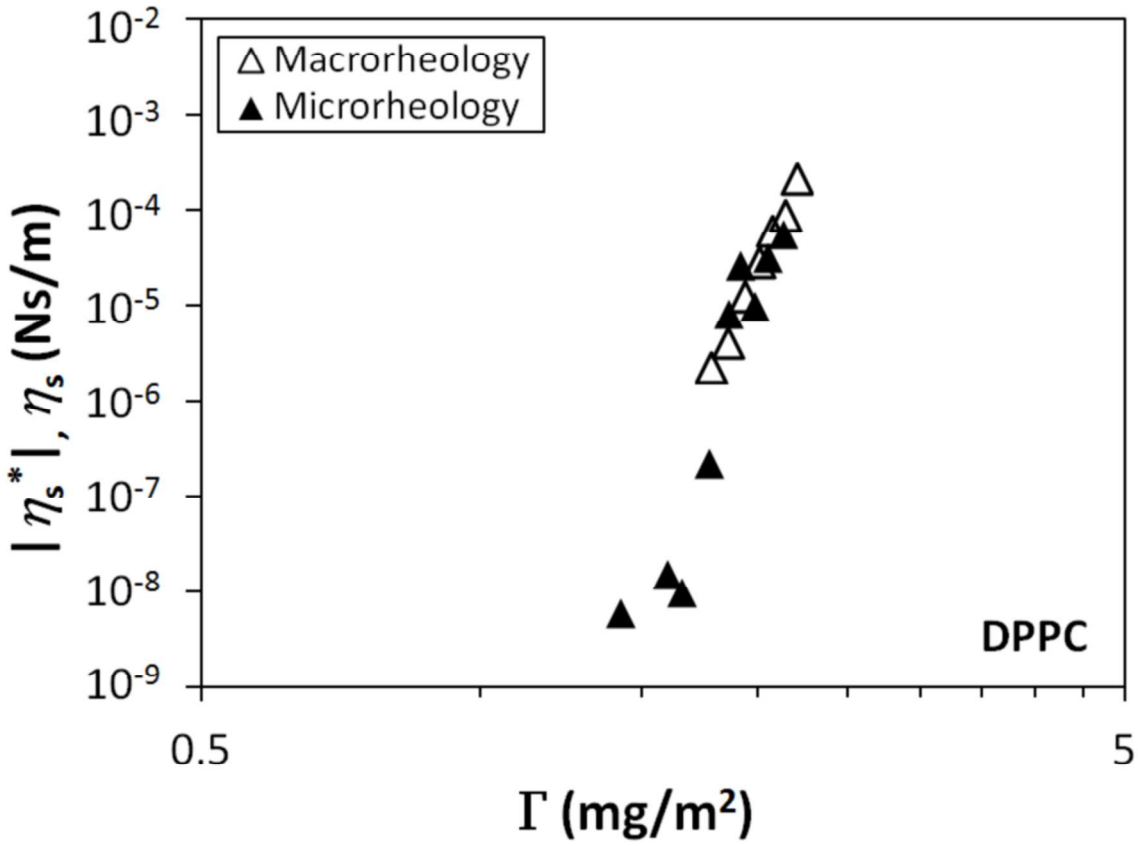

Figure 8. Surface viscosity as a function of surface coverage for DPPC. Microrheological results (▲) agree well with macrorheological results (△).

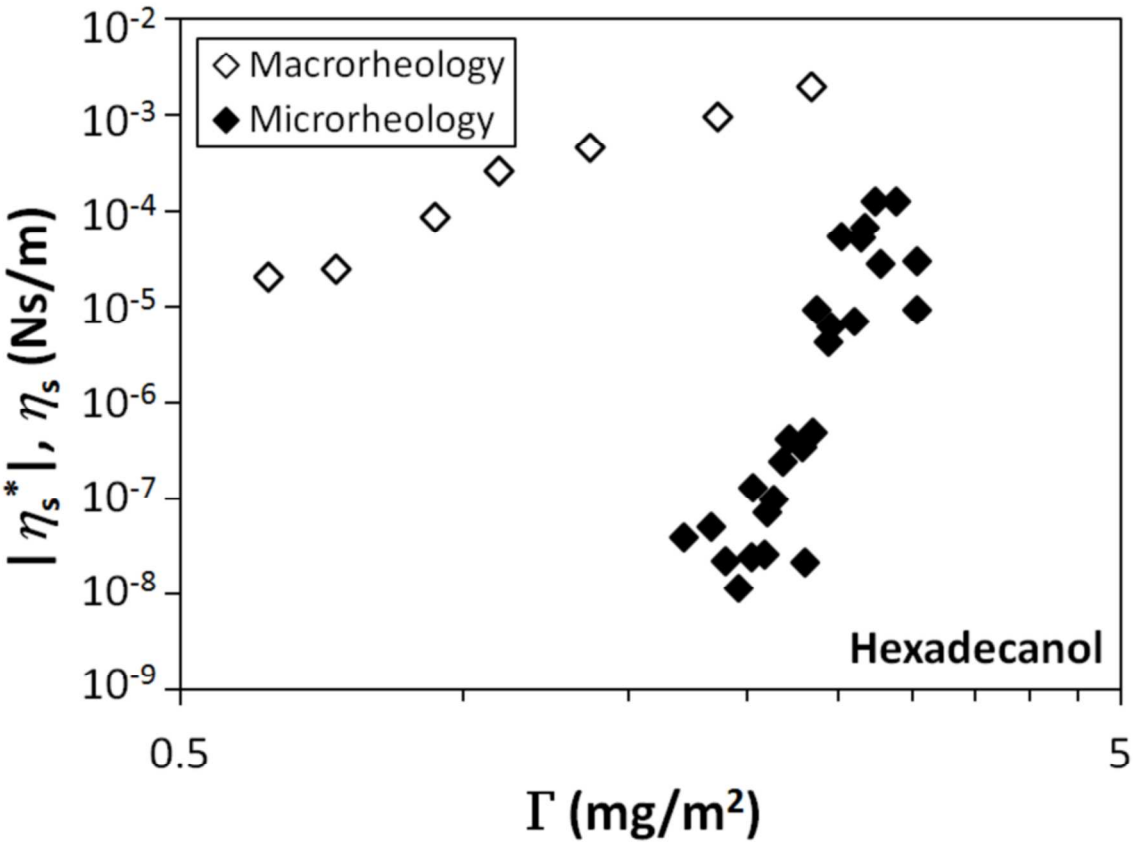

Figure 9. Surface viscosity as a function of surface coverage for hexadecanol. Microrheological results (◆) disagree with macrorheological results (◇) in both magnitude and trend.

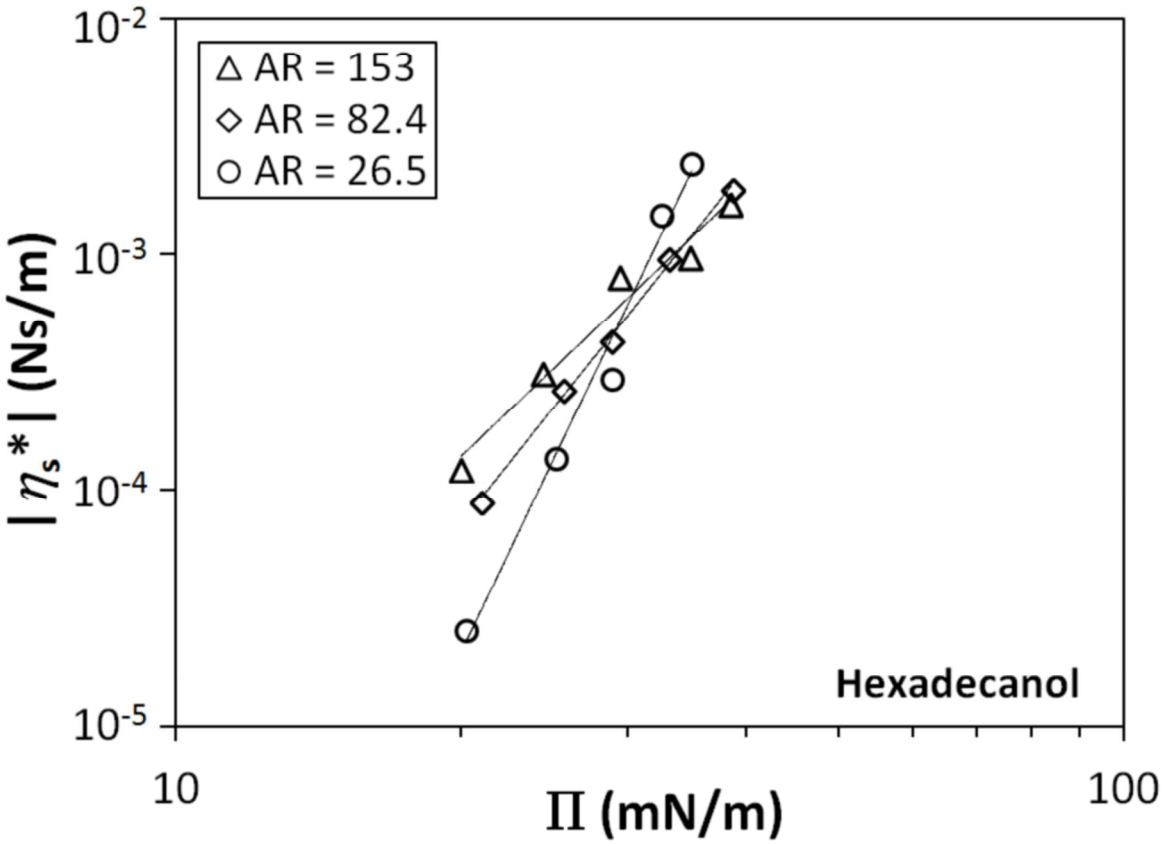

Figure 10. Complex surface viscosity as a function of Π, measured in the ISR for the hexadecanol system. Each data set comes from otherwise identical experiments using magnetic needles of different aspect ratio (AR), as reported in Table 1. Solid lines represent power-law fits to the data.

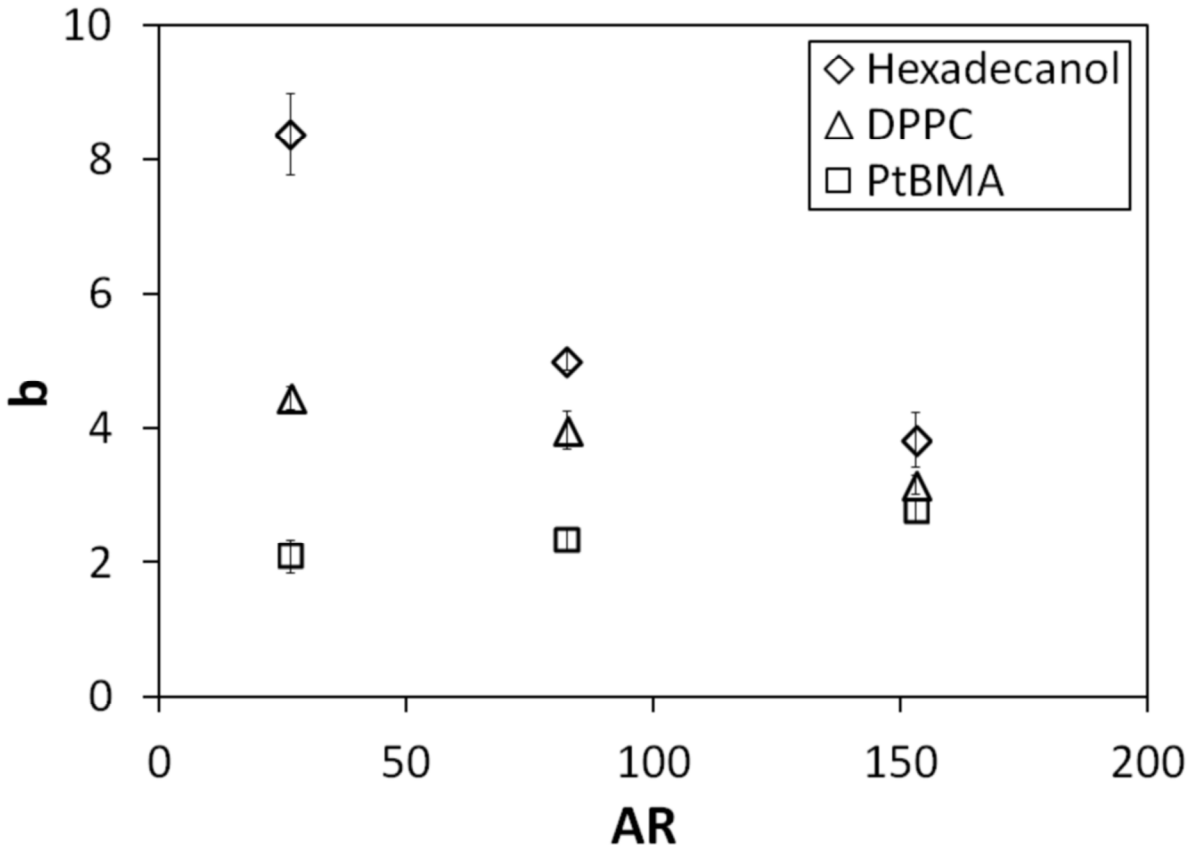

Figure 11. The exponent, b, calculated from fits of eq. 8 to $|\eta_s^*|$ vs Π data (Fig. 10) as a function of needle aspect ratio (AR). Results are shown for PtBMA, hexadecanol, and DPPC and an air-water interface.